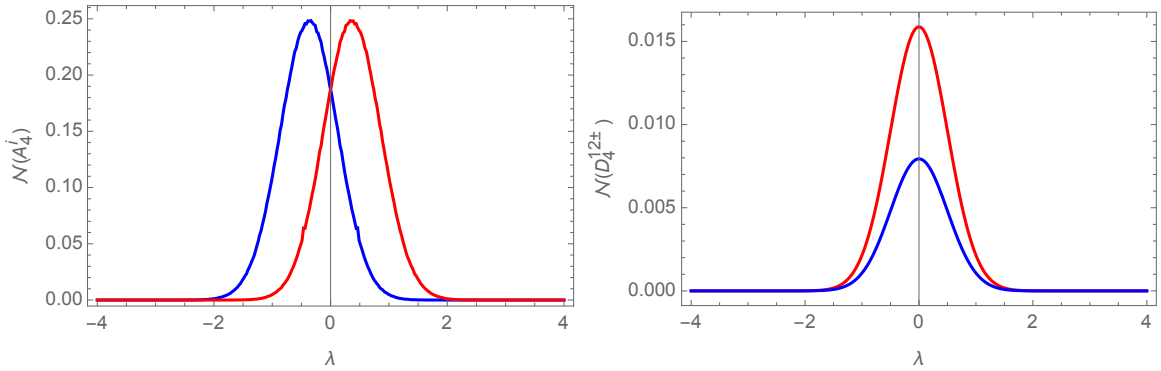

(a) The swallowtail number density $\mathcal{N}(A_4^i)$ corresponding to the first and the second eigenvalue field (red) and the second eigenvalue field (blue).

(b) The number density $\mathcal{N}(D_4^{12-})$ and $\mathcal{N}(D_4^{12+})$ (blue), and $\mathcal{N}(D_4^{12\pm})$ (red) as a function of the field. The swallowtail caustics corresponding to eigenvalue λ.

Figure 7: The number densities corresponding to the clusters in the caustic skeleton.

The number density of umbilic points is given by the Gaussian distribution

$$\mathcal{N}(D_4^{12\pm}) = \left\langle |\det\left(\nabla(T_{11}-T_{22}),\nabla(T_{12})\right)|\,\delta^{(1)}(T_{11}-\nu)\delta^{(1)}(T_{11}-T_{22})\delta^{(1)}(T_{12})\right\rangle \mathrm{d}\nu \tag{5.46}$$

$$= \int_{1/b_+}^{\infty}\int |(T_{111}-T_{122})T_{122}-(T_{222}-T_{112})T_{112}| \tag{5.47}$$

$$\times\, p(T_{11}=\nu, T_{12}=0, T_{22}=\nu, T_{111}, T_{112}, T_{122}, T_{222})\mathrm{d}\nu \tag{5.48}$$

$$\propto e^{-\frac{2\nu^2}{\tau_2^2}} \tag{5.49}$$

using the fact that $T_{11} = T_{22}$ and $T_{12} = 0$ at the umbilic points. The sign of the caustic, corresponding to the sign of $\mathcal{S}_{\mathcal{M}}$ determines the integration domain. By symmetry it follows that the hyperbolic and elliptic caustics are equally likely to be realized, *i.e.*,

$$\mathcal{N}(D_4^{12\pm}) = 2\mathcal{N}(D_4^{12+}) = 2\mathcal{N}(D_4^{12-})\,. \tag{5.50}$$

5.4 Numerical example

We can study these statistics numerically for a realization of the density perturbation field. See figure 8 for the caustic skeleton in Lagrangian space corresponding to the realization presented in figure 2. See figure 9 geometrical properties of this realization of the caustic skeleton.

6 Constrained initial conditions

To study characteristic properties of the different elements of the cosmic web, in both Lagrangian and Eulerian space, we use constrained Gaussian random field theory. Unfortunately, we cannot directly use the constrained analysis discussed in section 2.3, as the caustic

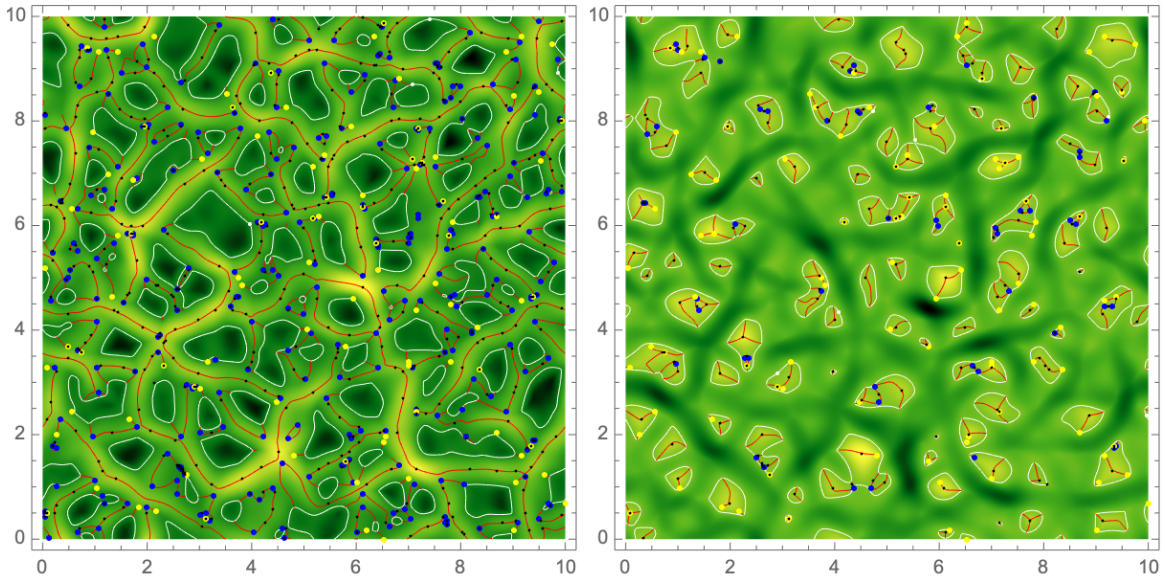

(a) The caustic skeleton corresponding to the first eigenvalue field λ_1

(b) The caustic skeleton corresponding to the second eigenvalue field λ_2

Figure 8: The caustic skeleton in Lagrangian space in a periodic 10 Mpc $\times$10 Mpc box with 2048 $\times$ 2048 grid points. The skeleton includes the shell-crossing curve A_2^i corresponding to $b_+ \to \infty$ (white), the cusp curve A_3^i (red), cusp points $A_3^{i\pm}$ (black), the swallowtail points A_4^i (blue), and the umbilic points D_4^{12}.

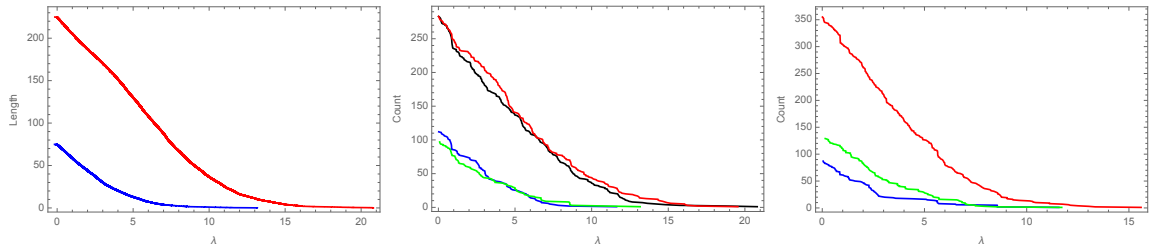

(a) The length of the A_3 lines as a function of the eigenvalue. The length $\mathcal{L}(A_3^1)$ in red and $\mathcal{L}(A_3^2)$ in blue.

(b) The number of $A_3^{\pm}$ points as a function of the eigenvalue. The density of A_3^{1+} (black), A_3^{1-} (red), A_3^{2+} (blue), and A_3^{2-} (green) points.

(c) The number of A_4^1 (red), A_4^2 (blue), and D_4^{12} (green) points as a function of the eigenvalue.

Figure 9: The statistics of the caustic skeleton in Lagrangian space as a function of the eigenvalue field.

conditions are non-linear functionals of the Gaussian deformation potential. For this reason, consider the constraint manifold $\mathcal{M}_\mathcal{C}$ defined by the caustic conditions in the space of derivatives of the deformation potential

$$\mathcal{M}_\mathcal{C} = \{(T_{ij\ldots})|\mathcal{C}_j[\lambda_i, \boldsymbol{v}_i; \boldsymbol{x}_j] = 0, \text{ for } j = 1, 2, \ldots, n\}\,, \tag{6.1}$$

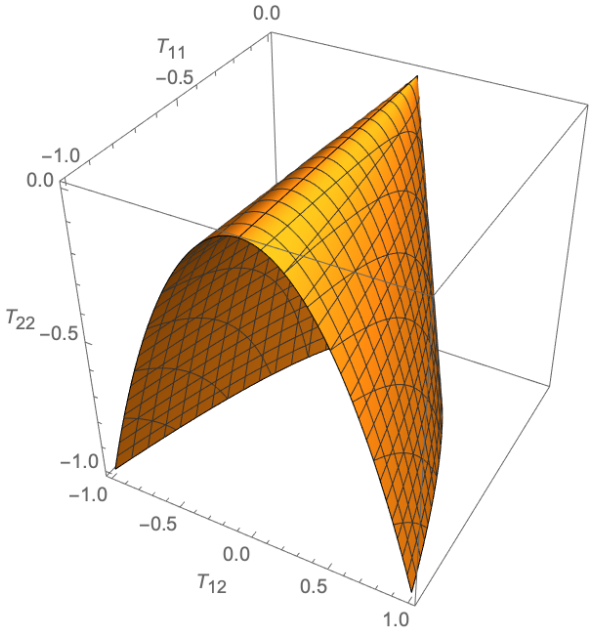

Figure 10: The constraint manifold $\mathcal{M}_{\mathcal{C}}$ in the space of derivatives of the deformation tensor corresponding to equation (6.2).

with the n non-linear constraints $\mathcal{C}_i$ implementing the caustic conditions. For example, the condition on the first eigenvalue field $\mathcal{C}_1(\lambda_i, \boldsymbol{v}_i) = \lambda_1 - \nu$ defines the constraint surface

$$\mathcal{M}_{\mathcal{C}} = \left\{ (T_{11}, T_{12}, T_{22}) \middle| \nu = \frac{1}{2}\left(T_{11} + T_{22} + \sqrt{4T_{12}^2 + (T_{11} - T_{22})^2} \right) \right\} \subset \{(T_{11}, T_{12}, T_{22})\}\,. \tag{6.2}$$

See figure 10 for an illustration. It follows from Bayes rule that the distribution of points on the constraint manifold $\boldsymbol{c} \in \mathcal{M}_{\mathcal{C}}$ is proportional to the original Gaussian distribution

$$p(\boldsymbol{c}|\boldsymbol{c} \in \mathcal{M}_{\mathcal{C}}) = \frac{p(\boldsymbol{c})}{\int_{\mathcal{M}_{\mathcal{C}}} p(\boldsymbol{c}) \mathrm{d}\boldsymbol{c}}\,. \tag{6.3}$$

An instance $\boldsymbol{c} \in \mathcal{M}_{\mathcal{C}}$ of this distribution, defines a set of linear constraints C_i on the derivatives of the deformation potential being used in the constraint manifold. For example, a instance $\boldsymbol{c}$ on the manifold manifold (6.2) defines three linear constraints $C_1[\Psi] = T_{11}, C_2[\Psi] = T_{12}, C_3[\Psi] = T_{22}$, with a corresponding mean field

$$\bar{\Psi}_{\boldsymbol{c}} = \sum_{i,j=1}^{n} \xi_i(\boldsymbol{q}) \xi_{ij}^{-1} c_i \tag{6.4}$$

and a residue Ψ_n with the variance

$$\left\langle \Psi_n(\boldsymbol{q})^2 | C_i[\Psi; \boldsymbol{q}_i] \right\rangle = \tau_0^2 - \sum_{i,j=1}^{n} \xi_i(\boldsymbol{q}) \xi_{ij}^{-1} \xi_j(\boldsymbol{q})\,. \tag{6.5}$$

We can use the Hoffman-Ribak method (algorithm 2) to construct a realization of the constrained Gaussian random field corresponding to this instance $\boldsymbol{c}$.

Conversely, given the mean field $\bar{\Psi}_{\boldsymbol{c}}$ corresponding to the instance $\boldsymbol{c} \in \mathcal{M}_{\mathcal{C}}$, we can evaluate the mean field corresponding to the constraints $\mathcal{C}$ by integrating over the constraint manifold, *i.e.*,

$$\begin{aligned}
\bar{\Psi}_{\mathcal{C}}(\boldsymbol{q}) &= \langle \Psi(\boldsymbol{q}) | \mathcal{C} \rangle && (6.6)\\
&= \int_{\boldsymbol{c} \in \mathcal{M}_{\mathcal{C}}} \bar{\Psi}_{\boldsymbol{c}}(\boldsymbol{q}) p(\boldsymbol{c} | \boldsymbol{c} \in \mathcal{M}_{\mathcal{C}}) \mathrm{d}\boldsymbol{c} && (6.7)\\
&= \sum_{i,j=1}^{n} \xi_i(\boldsymbol{q}) \xi_{ij}^{-1} \int_{\boldsymbol{c} \in \mathcal{M}_{\mathcal{C}}} c_i p(\boldsymbol{c} | \boldsymbol{c} \in \mathcal{M}_{\mathcal{C}}) \mathrm{d}\boldsymbol{c} && (6.8)\\
&= \sum_{i,j=1}^{n} \xi_i(\boldsymbol{q}) \xi_{ij}^{-1} \bar{c}_i && (6.9)\\
&= \bar{\Psi}_{\bar{\boldsymbol{c}}}(\boldsymbol{q}) \,, && (6.10)
\end{aligned}$$

where

$$\bar{\boldsymbol{c}} = \langle \boldsymbol{c} | \mathcal{C} \rangle = \int_{\boldsymbol{c} \in \mathcal{M}_{\mathcal{C}}} \boldsymbol{c}\, p(\boldsymbol{c} | \boldsymbol{c} \in \mathcal{M}_{\mathcal{C}}) \mathrm{d}\boldsymbol{c} \,. \tag{6.11}$$

The variance of the corresponding residue coincides with the variance of the field with the linear constraints,

$$\left\langle \Psi_n(\boldsymbol{q})^2 | \mathcal{C} \right\rangle = \tau_0^2 - \sum_{i,j=1}^{n} \xi_i(\boldsymbol{q}) \xi_{ij}^{-1} \xi_j(\boldsymbol{q}) \,, \tag{6.12}$$

since the variance of the sum of two distributions is the sum of the variances and the variance $\langle \Psi_n^2 | C_i = c_i \rangle$ is independent of values c_i. This property is special to the Gaussian statistics. Using this prescription we can evaluate the mean deformation potential of the filaments, clusters and Morse points at which the topology of the caustic skeleton changes.

6.1 Cusp caustics

The cusp filaments are defined by the conditions $\lambda_i = \nu$ and $\boldsymbol{v}_i \cdot \lambda_i = 0$, corresponding to the constraint manifold

$$\mathcal{M}_{\mathcal{C}} = \{(T_{11}, T_{12}, T_{22}, T_{111}) = (\nu_1, 0, \nu_2, 0) | \nu_1 \geq \nu_2\}. \tag{6.13}$$

In the eigenframe of the deformation tensor, the constraints for the A_3^1 caustic take the simple form

$$C_1[\Psi; \mathbf{0}] = T_{11} \,, \quad C_2[\Psi; \mathbf{0}] = T_{22} \,, \quad C_3[\Psi; \mathbf{0}] = T_{12} \,, \quad C_4[\Psi; \mathbf{0}] = T_{111} \,, \tag{6.14}$$

with $\bar{\boldsymbol{c}} = (\lambda, \bar{c}_2(\lambda), 0, 0)$, where the average second constraint is given by the identity

$$\begin{aligned}
\bar{c}_2(\lambda) &= \int_{\mathcal{M}_{\mathcal{C}}} T_{22}\, p(T_{11} = \lambda, T_{22}, T_{12} = 0, T_{111} = 0 | T_{11} = \lambda, T_{12} = 0, T_{111} = 0) \mathrm{d}T_{12} && (6.15)\\
&= \frac{\lambda}{3} + \tau_2^2 \frac{\mathrm{Erfc}\left[\sqrt{\frac{2}{3}} \frac{\lambda}{\tau_2}\right] - 2}{\sqrt{\frac{6}{\pi}} \tau_2 e^{-\frac{2\lambda^2}{3\tau_2^2}} - 2\lambda \left(\mathrm{Erfc}\left[\sqrt{\frac{2}{3}} \frac{\lambda}{\tau_2}\right] - 2\right)} \,. && (6.16)
\end{aligned}$$

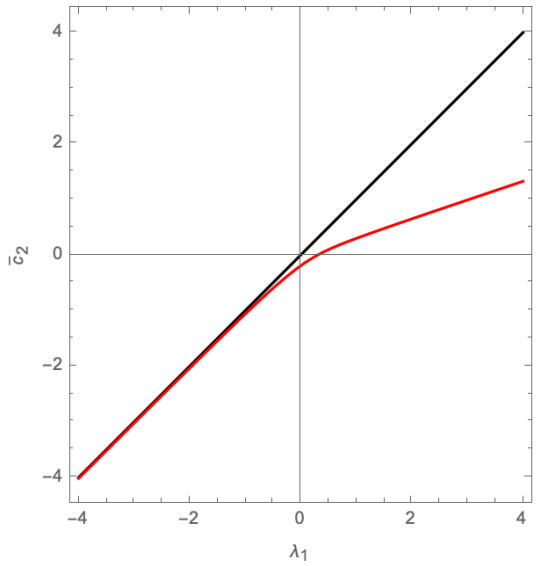

Figure 11: The mean constraint $\bar{c}_2$ for the cusp filament for $\alpha = 1$ and $R = 1$.

See figure 11 for an illustration of the mean constraint $\bar{c}_2$.

The mean deformation potential for the cusp filament $\bar{\Psi}_{\bar{\boldsymbol{c}}}(\boldsymbol{q})$ in the initial conditions, for the power-law power spectrum smoothed by a Gaussian is given by

$$\bar{\Psi}_{\bar{\boldsymbol{c}}}(\boldsymbol{q}) = -2e^{-\frac{q^2}{8R^2}} R^2 \left((\bar{c}_2(\lambda) + \lambda) I_0 \left[\frac{q^2}{8R^2} \right] + 2(\bar{c}_2(\lambda) - \lambda) I_1 \left[\frac{q^2}{8R^2} \right] \cos(2\theta) \right) . \tag{6.17}$$

See figure 12 for an illustration of the mean field and the variance of the residue near the constraint.

Now we consider the distribution of $\nabla(\boldsymbol{v}_i \cdot \nabla\lambda_1)$ in order to obtain the average initial conditions under the condition that the filament has a given orientation. Note that

$$\boldsymbol{v}_1 \cdot \nabla(\boldsymbol{v}_1 \cdot \nabla\lambda_1) = T_{1111} + \frac{3T_{112}^2}{T_{11} - T_{22}} , \tag{6.18}$$

$$\boldsymbol{v}_2 \cdot \nabla(\boldsymbol{v}_1 \cdot \nabla\lambda_1) = T_{1112} + \frac{3T_{112}T_{122}}{T_{11} - T_{22}} . \tag{6.19}$$

In order to evaluate the distribution of the orientation, we need to study the statistics of the angle θ between $\boldsymbol{v}_1$ and $\nabla(\boldsymbol{v}_1 \cdot \nabla\lambda_1)$. This is completely described by $p(T_{11}, T_{22}, T_{112}, T_{122}, T_{1111}, T_{1112})$.

6.2 Umbilic caustics

The umbilic caustics are defined by the linear conditions

$$C_1[\Psi; \mathbf{0}] = T_{11} , \tag{6.20}$$

$$C_2[\Psi; \mathbf{0}] = T_{22} , \tag{6.21}$$

$$C_3[\Psi; \mathbf{0}] = T_{12} . \tag{6.22}$$

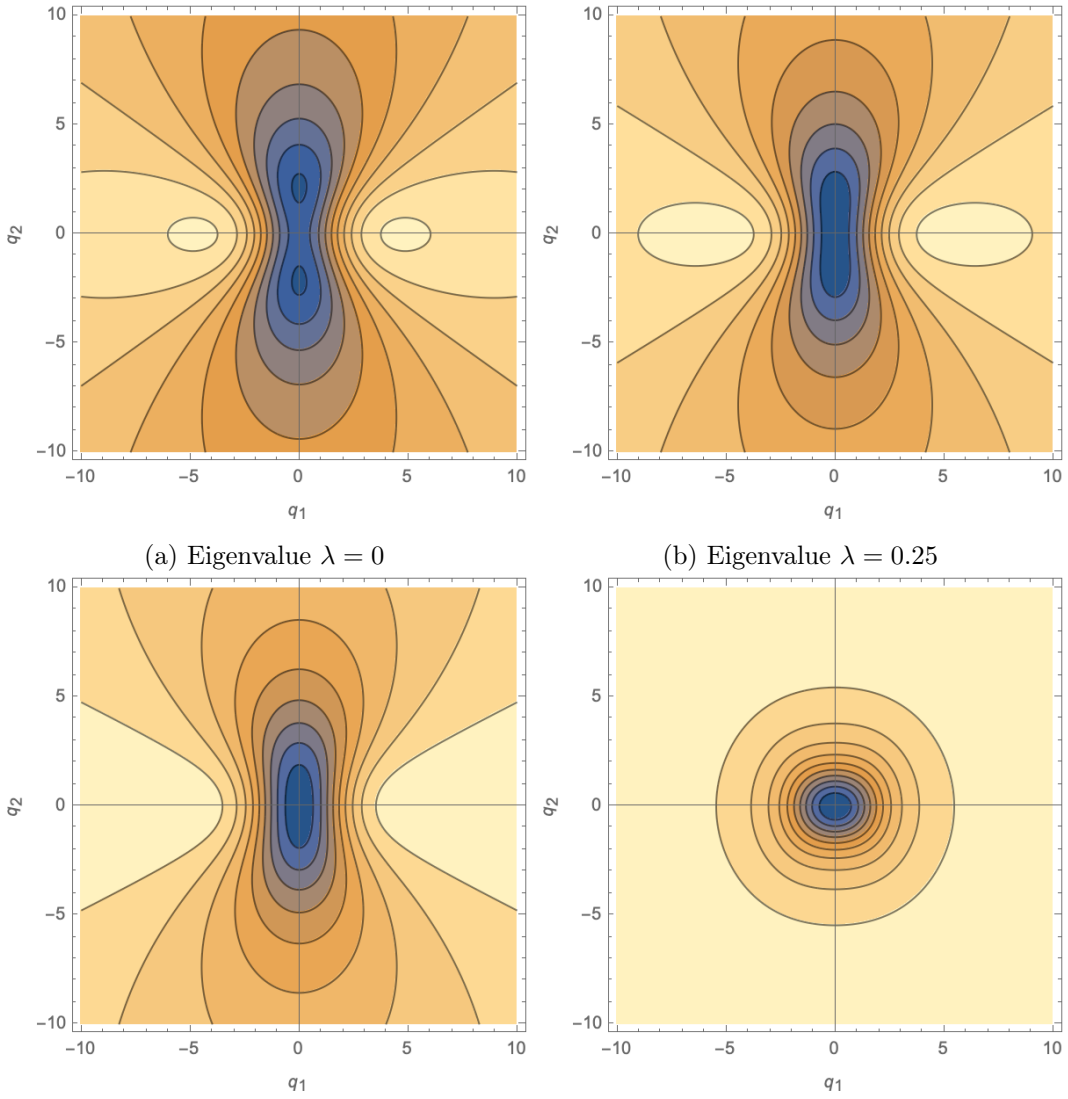

(a) Eigenvalue $\lambda = 0$

(b) Eigenvalue $\lambda = 0.25$

(c) Eigenvalue $\lambda = 0.5$

(d) Variance of the residue

Figure 12: The mean deformation potential for the cusp filament for $\alpha = 1$ and $R = 1$.

with $\boldsymbol{c} = (\nu, \nu, 0)$, which defines the constraint manifold

$$\mathcal{M}_{\mathcal{C}} = \{(T_{11}, T_{12}, T_{22}) | T_{11} = T_{22} = \nu, \text{ and } T_{12} = 0\}\,, \tag{6.23}$$

consisting of a single point.

The cross-correlation of the deformation potential with respect to the constraint is

$$\xi_1(\boldsymbol{q}) = -\frac{1}{2\pi}\int_0^\infty k^2 P_\Psi(k)\left(\frac{J_1(qk)}{qk} - J_2(qk)\right)\mathrm{d}k\,, \tag{6.24}$$

$$\xi_2(\boldsymbol{q}) = -\frac{1}{2\pi}\int_0^\infty k^2 P_\Psi(k)\frac{J_1(qk)}{qk}\mathrm{d}k\,, \tag{6.25}$$

$$\xi_3(\boldsymbol{q}) = 0\,, \tag{6.26}$$